Water Science & Technology

Water Science & Technology Vol 84 No 3, 697 doi: 10.2166/wst.2021.247

Efficient removal of acetic acid by a regenerable resin-based spherical activated carbon

Huiling Wu [a,b], Wenjing Sun[a], Huangzhao Wei[a], Ying Zhao[a], Chengyu Jin[a], Xu Yang[a], Xin Rong[a] and Chenglin Sun[a,*]

[a] Dalian Institute of Chemical Physics, Chinese Academy of Sciences, Dalian 116023, China
[b] University of Chinese Academy of Sciences, Beijing 100049, China
*Corresponding author. E-mail: clsun@dicp.ac.cn

HW, 0000-0003-1428-2806

ABSTRACT

Carboxylic acids are the main pollutant of industrial wastewater during the advanced oxidation process (AOPs). In this study, a resin-based spherical activated carbon (RSAC, AF_5) as an adsorbent was examined and acetic acid was used as a model substrate for adsorption investigation. The pH = 3, temperature = 298 K were fixed by batch technique. The pseudo-second-order kinetic model, the intraparticle and external models are fitted well, and it was found that the adsorption of acetic acid onto AF_5 was controlled by liquid film diffusion. A Freundlich model indicated that the adsorption process was heterogeneous multimolecular layer adsorption on the surface. AF_5 shows good regenerative ability; the recovery rate of adsorption capacity was ~88% after five cycles. Chemical oxygen demand (COD) adsorption removal rate could be maintained at 100% for over 35 h in an actual AOPs effluent, and could be eluted for 100% after 8 h by 0.8wt% NaOH. Characterizations, including XRF, XRD, TG/DSC,FTIR, SEM and N_2 adsorption, showed that the excellent adsorption performance was mainly due to the microporous structure and large specific surface area (1,512.88 m^2/g), the adsorption mechanism mainly included pore filling effect and electrostatic attraction. After five adsorption recycles, AF_5's pore characteristic did not change significantly. This study provides a scientific basis for the wastewater standard discharge process of AOPs coupled adsorption.

Key words: acetic acid, adsorption, model fitting, resin-based spherical activated carbon, water treatment

HIGHLIGHTS

- The reusability of the acetic acid wastewater was increased by adsorption methods.
- Resin-spherical activated carbon was used as an adsorbent in acetic acid diluent.
- Freundlich isotherm and pseudo-second-order adsorption kinetics were the most suitable models.
- The effluent of CWAO/adsorption process effluent could reach the discharge standard.

GRAPHICAL ABSTRACT

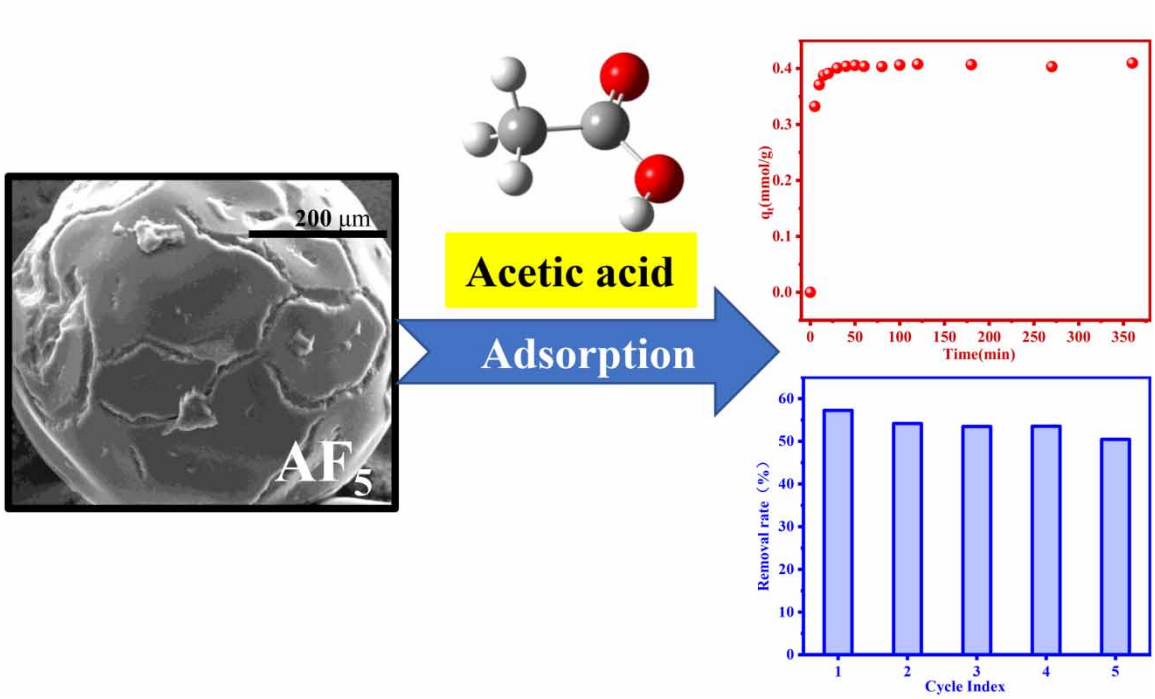

1. INTRODUCTION

The advanced oxidation process (AOPs) is industrially used for the treatment of wastewater, including to generate strong oxidizing free radicals that attack contaminants and break the chemical bonds. However, it is difficult to completely mineralize organic compounds into CO_2 and H_2O (Akbari *et al.* 2018; Gonzalez *et al.* 2020; Sanchez-Montes *et al.* 2020). Water effluent contains carboxylic acids, such as acrylic acid, oxalic acid, and acetic acid (Wang *et al.* 2017; Sun *et al.* 2019). To meet the 'zero discharge' of wastewater, a coupling process is usually required after AOPs. Biochemical treatment is commonly reported at present, However, some issues are raised subsequently, such as large floor areas, the mass of sludge produced, or seasonal production compared with its extension (Amor *et al.* 2019). Membrane treatment is also one of the common methods used, but the chemical oxygen demand (COD) of the influent must be lower than 80 mg/L and has a strict requirement for AOPs (Shi *et al.* 2020). In comparison, the adsorption method has attracted substantial attention because of its low energy consumption, high efficiency, and low cost (Herbert *et al.* 2020).

Acetic acid is a typical representative substance in the AOP effluent, to attain the discharge standard of AOP effluent, the removal of acetic acid by the adsorption method is a direct method. At present, various adsorbents have been reported for acetic acid. Xianghai Guo *et al.* used different kinds of water-tolerable metal–organic frameworks to systematically study the adsorptive activities for dilute acetic acid solutions, like MIL-derived and UiO-66-derived materials (Zhang *et al.* 2016; Yu *et al.* 2019). However, the high cost, the difficulty in large-scale industrial production, and poor thermal and chemical stability generate for MOFs materials many restrictions on their industrial application. Naidu and Mathews discussed the adsorption effect of acetic acid in the fermentation broth onto weakly base resin (Naidu & Mathews 2019), exchange amount is limited and the mechanical strength is low. More importantly, in these reports, the concentration range of acetic acid was mostly 1 wt%–4 wt%. For the effluent of AOPs, the total organic carbon (TOC) value is lower than 5,000 mg/L, and the acetic acid concentration is lower than 1wt%. Generally, the lower the concentration, the more difficult it is to adsorb for the smaller driving force. Therefore, it is important to explore an adsorbent with excellent adsorption and removal capacity for acetic acid diluent.

Carbon-based adsorbents, such as activated carbon, carbon nanotubes, carbon black, or carbon fiber are usually considered as the best adsorbents, and have been used for more than 2000 years in the adsorption process (Tagliavini *et al.* 2017).

Activated carbon is one of the most widely used materials due to its novel microporous structure and specific surface area. However, activated carbon with vast impurities and ash can no longer meet the needs for industrial applications (He *et al.* 2017). Compared to powder activated carbon (PAC) and granular activated carbon (GAC), the spherical shape of activated carbon spheres (SAC) makes it possible to prepare adsorbent particles of appropriate hydrodynamic properties. In the adsorption process, it has unique advantages of smaller ash content, lower pressure loss, higher fluidity, bulk density, and so on (Kameda *et al.* 2020).

Resin-based activated carbon spheres (RSACs) were prepared by the pyrolysis and carbonization of phenolic resin or ion exchange resin under an inert atmosphere at a certain temperature (Zhang *et al.* 2018). RSAC has exhibited good performance for the adsorption of pollutants. For example, RSAC prepared by suspension polymerization of alkylphenol and formaldehyde, steam activation in combination with surface modification by heat treatment with dry air, has an excellent capacity for Hg^0 adsorption (Zhang *et al.* 2018). Furthermore, Jun-Bing Yang *et al.* reported that RSAC, prepared by carbonization and steam activation of novolac-type phenolic resin with different pore-forming agents, also exhibited good VB_{12} adsorption properties (Yang *et al.* 2002).

In this paper, we describe RSAC as an excellent adsorbent for carboxylic acids, using acetic acid as the representative carboxylic acid. By single-factor experiments, kinetics and adsorption–desorption isotherm experiments, adsorption–elution experiments on actual wastewater, and recycling experiments for RSAC, the feasibility of RSAC as a stable and efficient adsorbent for the removal of acetic acid diluent was discussed. At the same time, through discussion of the characterization results of RSAC and adsorption mechanism, this study guides the development of alternative products.

2. MATERIALS AND METHODS

2.1. Experimental materials

Acetic acid (CH_3COOH, analysis grade) was purchased from Shanghai Aladdin Biological Technology Co., Ltd. Sodium hydroxide (NaOH, analysis grade), and sodium chloride (NaCl, analysis grade) were purchased from Tianda Chemical Reagent Factory, Dongli District, Tianjin. Hydrochloric acid (HCl, analysis grade) was purchased from Xinxing Reagent Co., Liaoning. Coconut shell activated carbon was purchased from Suzhou Taimei Activated Carbon Co., Ltd. The RSAC for this study called AF_5, purchased from Germany, has a burnish finish, and a homogeneous globular diameter of 400 to 800 μm. The composition was analyzed by X-ray fluorescence spectroscopy (XRF), shown in Table 1.

2.2. Characterization

The specific surface area and pore sizes were determined using physical adsorption apparatus (Quadrasorb SI type, Quanta-Chrome). The chemical composition of AF_5 was determined by X-ray fluorescence spectroscopy (Zetium model, PANalytical Company). An X-ray diffractometer (XRD, X'pert Pro-1 model, PANalytical Company) was used to analyze the structure and crystal form. The functional group types on the material's surface were analyzed by Fourier Transform infrared spectrometer (Varian 3100, Varian Company). The surface and section morphology was observed by high-resolution scanning electron microscopy (S5500) and scanning electron microscopy (JSM6360LV). Thermogravimetric analysis was performed using a TGA instrument (Netzsch STA 449 F3), the material was heated under a nitrogen atmosphere.

2.3. Batch adsorption experiment

Batch adsorption measurements for different concentrations of acetic acid were carried out in 100 mL corked conical flasks. In a 25 mL solution, 0.6 g AF_5 was added, and the pH of the solution was adjusted with HCl (1 mol/L) and NaOH (1 mol/L). The background electrolyte solution was 0.015 mol/L NaCl solution. The conical flask was placed in a 200 rpm/min constant temperature shaking box and oscillated at a steady temperature. After adsorption, the samples were filtered through a 0.45 μm filter, and the concentration of acetic acid in solution was analyzed by the Shimazu TOC-V analyzer. The effects of pH (1–10), adsorption temperature (298 K–308 K), adsorption time (0–360 min), initial concentration (200–2,000 mg/L) were

Table 1 | The elemental composition of AF_5

Elements	C	O	S	Ca	P	Ti	Fe	Al	Na	Others
Content (wt%)	93.340	3.288	1.262	0.659	0.439	0.317	0.251	0.117	0.105	0.222

investigated. For desorption experiments, the filtered adsorbent was collected and 25 mL 0.015 mol/L NaCl with pH = 3.0 was added for desorption. The amount of acetic acid adsorbed and desorbed can be calculated by the difference in acetic acid content before and after adsorption and desorption experiments, respectively. The adsorption capacity q_e could be calculated as following Equation (1):

$$q_e = \frac{(C_0 - C_t)V}{Mm} \tag{1}$$

where q_e is the adsorption capacity (mmol·g^{-1}), C_0 is the initial concentration (mg·L^{-1}), C_t is the adsorption solution concentration (mg·L^{-1}), V is the solution volume (L), and m is the adsorbent mass (g), and M is the relative molecular mass of acetic acid.

2.4. Adsorption model

2.4.1. Adsorption kinetic model

In the study, the experimental data were fitted using different adsorption kinetic models and the calculation formulas for these models are listed in Table 2.

Generally, the pseudo-first-order model only had a good fitting to data at the initial stage of the experiment and had a low matching degree for the entire adsorption experiment. Differently, the pseudo-second-order model can better fitted to the data and explain the adsorption mechanism for the whole adsorption process. The Elovich equation was suitable for adsorption determined by composite mechanism. Based on the assumption of the Weber–Morris model, when the fitted curve crosses the origin, the only rate-limiting step was the intraparticle diffusion; otherwise, the adsorption process was controlled by both internal and external diffusion (Cherkasov 2020). For the Boyd model, if the line between t and B_t crossed the origin, the adsorption was controlled by intraparticle diffusion. If not, liquid-film controlled.

2.4.2. Adsorption isotherm model

In this paper, the experimental data were fitted using the following isotherm models, and the calculation formulas of those models are listed in Table 3.

The Freundlich model is an empirical formula for multimolecular layer adsorption based on a collection of experimental results. These could be used to describe non-ideal adsorption and multilayer adsorption on non-uniform surfaces and are suitable for various physical and chemical adsorption behaviors. The Langmuir model describes the monolayer adsorption equilibrium theory proposed by Langmuir. It is assumed that the surface of adsorbents was homogeneous and no interaction between adsorbents occurs. For $K_L \cdot C_e \ll 1$ in Langmuir and $n = 1$ in the Freundlich model, the saturation of the adsorbent was much higher than the maximum equilibrium capacity reached experimentally, none of the Langmuir and Freundlich models could be used because both models reduced to a linear isotherm under the particular conditions, adsorbate had a linear distribution on the adsorbent. The Temkin model assumes that the surface of the adsorbent is uniform and ideal with uniform distribution and the same adsorption energy of each adsorption site.

Table 2 | Kinetic models

Equation	Plot	Constants	Equation number
Pseudo-first-order model $q_t = q_e(1 - e^{-K_1 t})$	q_t versus t	K_1, q_e	(2)
Pseudo-second-order model $q_t = K_2 q_e^2 t/(1 + K_2 q_e t)$	q_t versus t	K_2, q_e	(3)
Elovich equation $q_t = A + B \ln t$	q_t versus t	A, B	(4)
Weber–Morris intraparticle diffusion models $q_t = K_{ipd} t^{\frac{1}{2}} + C$	q_t versus $t^{1/2}$	K_{ipd}, C	(5)
Boyd model $B_t = -0.4977 - \ln(1 - q_t/q_e)$	B_t versus t	q_e	(6)

In these equations, q_t – instantaneous adsorption capacity, mmol·g^{-1}. q_e – the amount of adsorption at equilibrium, mmol·g^{-1}.
In Equations (2) and (3), K_1 (min^{-1}), K_2 (g·mmol^{-1}·min^{-1}) – the rate constants of pseudo-first-order, pseudo-second-order kinetic models respectively.
In Equation (4), A and B are the correlation constants in the Elovich equation.
In Equation (5), K_{ipd} – a rate constant of Weber–Morris intraparticle diffusion, mmol·g^{-1}·min$^{-1/2}$. C – the constant. The greater the C, the more the boundary layer affects the adsorption process.
In Equation (6), B_t is the function of the Boyd model.

Table 3 | Isotherm models

Equation	Plot	Constants	Equation number
Freundlich model $q_e = K_F \times C_e^{\frac{1}{n}}$	q_e versus C_e	K_F, n	(7)
Langmuir model $q_e = K_L Q_m C_e/(1 + K_L C_e)$	q_e versus C_e	K_L, Q_m	(8)
Temkin model $q_e = RT/b_T \times \ln K_T C_e$	q_e versus C_e	b_T, K_T	(9)

In Equations (7)–(9), q_e – the solid phase adsorption amount of the pollutant at adsorption equilibrium (mmol·g^{-1}). C_e – the liquid phase concentration of solution at adsorption equilibrium (mmol·L^{-1}).
In Equation (7), K_F-(mg·g^{-1})(L·mmol^{-1})$^{-1/n}$, n – equilibrium constant of Freundlich model, expresses the adsorption capacity of the adsorbent, represents the adsorption strength or non-uniformity of the adsorbent.
In Equation (8), Q_m – the maximum adsorption capacity (mmol·L^{-1}); K_L – the equilibrium constant of the Langmuir model (L·mmol^{-1}).
In Equation (9), b_T – Temkin constant, kJ·mol^{-1}; K_T – Temkin model equilibrium constant (L·mmol^{-1}); R – gas constant, 8.314 (J·mol^{-1}·K^{-1}); T – absolute temperature, K.

The applicability of those models was evaluated from the determination coefficient values (R^2) and normalized standard deviation Δq_e(%). The Δq_e values were calculated according to Equation (10):

$$\Delta q_e(\%) = 100 * \sqrt{\frac{\sum \left[\frac{q_{e,\exp} - q_{e,cal}}{q_{e,\exp}}\right]^2}{N-1}} \tag{10}$$

where, $q_{e,\exp}$ and $q_{e,cal}$ are the experimental and calculated adsorption capacity (mmol·g^{-1}) respectively, and N is the number of adsorption essays. For the desorption experiments, ΔC_e(%) was used to indicate the isotherm model applicability. The ΔC_e(%) value was calculated according to Equation (11):

$$\Delta C_e(\%) = 100 * \sqrt{\frac{\sum \left[\frac{C_{e,\exp} - C_{e,cal}}{C_{e,\exp}}\right]^2}{N-1}} \tag{11}$$

where, $C_{e,\exp}$ and $C_{e,cal}$ are the experimental and calculated solution concentration (mol·L^{-1}) respectively, and N is the number of adsorption essays.

3. RESULTS AND DISCUSSION

3.1. Adsorption influencing factors

3.1.1. Effect of pH

Since the pH of the solution changed the charge of the adsorbent and adsorbate, the adsorption of acetic acid on AF_5 was strongly dependent on the pH variation. The study was carried at pH ranging from 1.5 to 10 maintaining other parameters constant, and the results are shown in Figure 1(a). The removal rate of acetic acid was gradually increased with the enhancement of pH value when it was lower than 3 and a maximum adsorption removal rate (58.64%) was obtained at pH = 3. Then, a sharp decrease in removal rate was occurred at a higher pH value and finally declined to almost zero when the solution was basic (pH = 6–10). This trend could be explained by the electrostatic interaction between the surface of AF_5 and acetic acid molecules. In further experiments, the pH was fixed at 3.

3.1.2. Effect of temperature

Temperature also affected the adsorption process. At different temperatures, the adsorption process of different concentrations of the acetic acid solution was investigated, and other conditions remained the same. The results are shown in Figure 1(b). For acetic acid diluents with different concentrations, the adsorption removal rate was higher at 298 K than at 308 K, indicating that the adsorption process was exothermic. So further experiments were conducted at 298 K only. For industrial application, the room temperature conditions were feasible without providing an additional heat source.

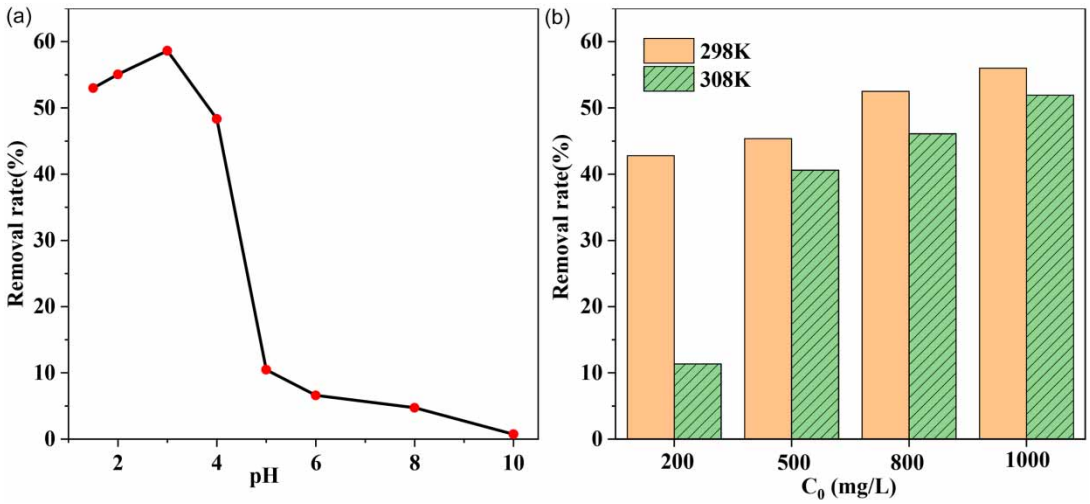

Figure 1 | (a) Effect of pH, conditions: 0.015 mol·L^{-1} NaCl, 200 rpm, contact time 3 h, 1,000 mg·L^{-1} acetic acid, AF_5 0.6 g/25 mL. (b) Effect of temperature, conditions: 0.015 mol·L^{-1} NaCl, 200 rpm, contact time 3 h, pH 3, AF_5 0.6 g/25 mL.

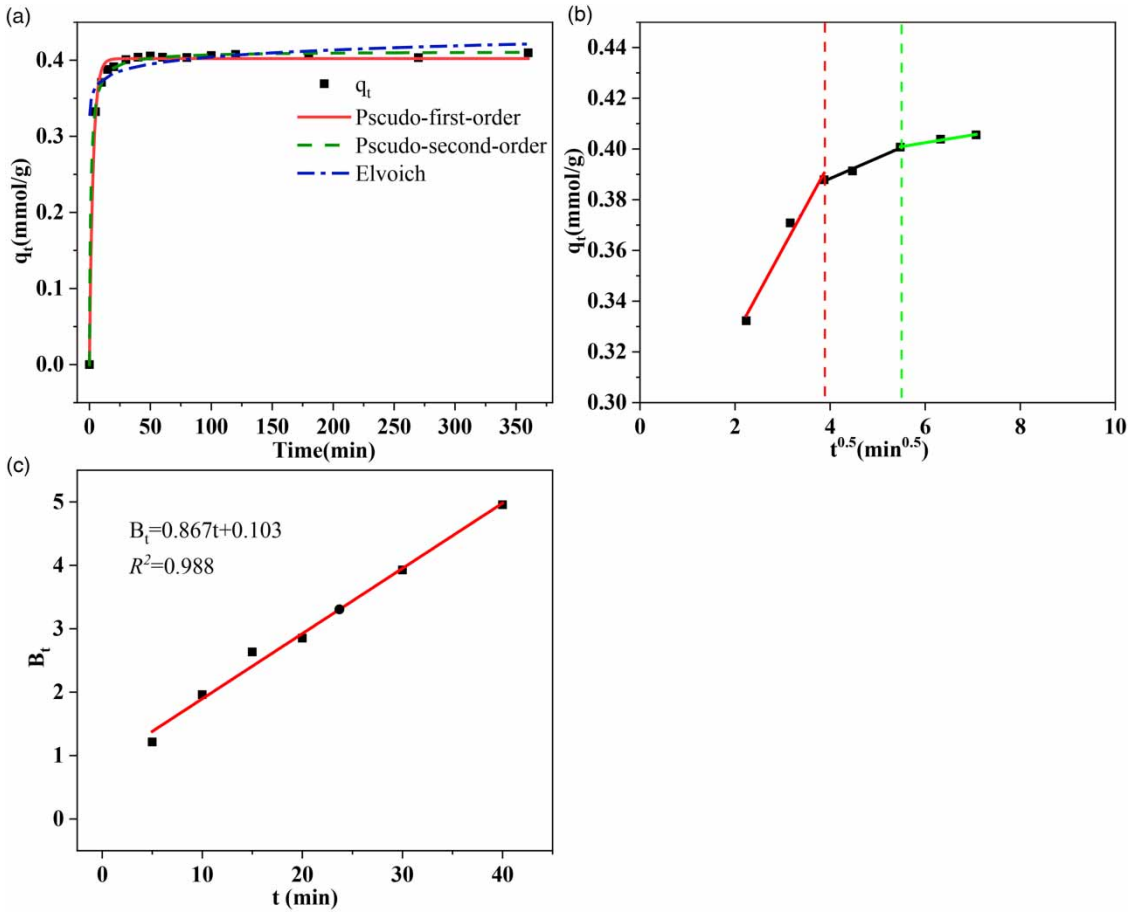

Figure 2 | (a) Kinetic curves of acetic acid on AF_5, (b) The Adsorption process fitted by intraparticle diffusion, (c) Linear fitting diagram between B_t and t.

3.2. Adsorption kinetics

3.2.1. Kinetic model fitting

To study the adsorption mechanism, kinetic adsorption experiments with 1,000 mg·L^{-1} of acetic acid solution were carried out at 298 K. The adsorption capacity of AF_5 was monitored at different times, and the adsorption kinetics is given in Figure 2(a). The amount of acetic acid adsorbed by AF_5 increases with time in the initial stage (<50 min). After 50 min, the adsorption kinetic curve tended to be flat, and the adsorption equilibrium for AF_5 was reached. According to the results of kinetic fitting (Table 4), the pseudo-first-order kinetic model and Elovich's kinetic equation exhibited good fitting (the correlation coefficient $R^2 > 0.98$). In comparison, the correlation coefficient (R^2) obtained by the pseudo-second-order kinetic model reached 0.999 and had a smaller Δq_e of 0.827 (Table 4). Therefore, the pseudo-second-order model was more suitable to describe the adsorption process, indicating the existence of both physical and chemical adsorption. Of note, the pseudo-second-order kinetic model should include external liquid film diffusion, surface adsorption, and intraparticle diffusion.

3.2.2. Diffusion mechanism

To describe the kinetic process, the Weber–Morris model was used to fit the kinetic data before the adsorption equilibrium (e.g. 0–50 min), as shown in Figure 2(b). Relevant parameters for the intraparticle diffusion model are given in Table 5. The partitioned linear relationship of q_t and $t^{0.5}$ indicated that the acetic acid adsorption over AF_5 was composed of multiple adsorption processes. The first stage was the rapid adsorption phase from 5 to 15 min, in which the adsorbent reached the AF_5's surface through the liquid film (involving surface adsorption). In the second stage (~15–30 min), the adsorbate diffused from the surface to the periphery of the pores and into the interior ultimately (i.e. the intraparticle diffusion stage). In the third stage (~30–50 min), the adsorbate is adsorbed at the activate site finally to achieve a balance between adsorption and desorption, that is the adsorption stage (Wang *et al.* 2020).

3.2.3. External diffusion model

Next, we applied Boyd's model to describe the adsorption process, as depicted in Figure 2(c). The relationship between B_t and t was linear, and the correlation coefficient R^2 was 0.988. The fitted curve did not pass the origin and the slope value B (0.867) was smaller than 1, meaning that the adsorption rate is mainly controlled by the liquid film diffusion. According to Weber–Morris intraparticle diffusion and Boyd's model, the adsorption kinetic should be mainly controlled by the liquid film diffusion, of note, and is also affected by intraparticle diffusion.

3.3. Adsorption isotherm

Furthermore, adsorption isotherms were used to study the distribution of the adsorbed molecules between the aqueous and solid phases under equilibrium conditions (Liang *et al.* 2018). Adsorption experiments were carried out at pH = 3 for 3 h.

It was found that the adsorbed amount of acetic acid on AF_5 increased with the increasing acetic acid concentration at 298 K, the Freundlich, Langmuir and Temkin models were used to fit the tested data, respectively (Figure 3(a)), and the fitting

Table 4 | Adsorption kinetic parameters of AF_5

Adsorption model	$q_{e,exp}$ (mmol·g^{-1})	$q_{e,cal}$ (mmol·g^{-1})	K	R^2	Δq_e (%)
Pseudo-first-order	0.406	0.402	0.329	0.995	1.945
Pseudo-second-order	0.406	0.412	2.180	0.999	0.827
	$q_{e,exp}$ (mmol·g^{-1})	A (mmol·g^{-1}·min^{-1})	B (g·mmol^{-1})	R^2	Δq_e (%)
Elvoich	0.406	0.342	0.013	0.986	3.431

Table 5 | Fitting parameters of intraparticle diffusion

	K_{ipd} (mmol·g^{-1}·min$^{-1/2}$)	C	R^2
First stage	0.034	0.258	0.959
Second stage	0.008	0.356	0.974
Third stage	0.003	0.384	0.968

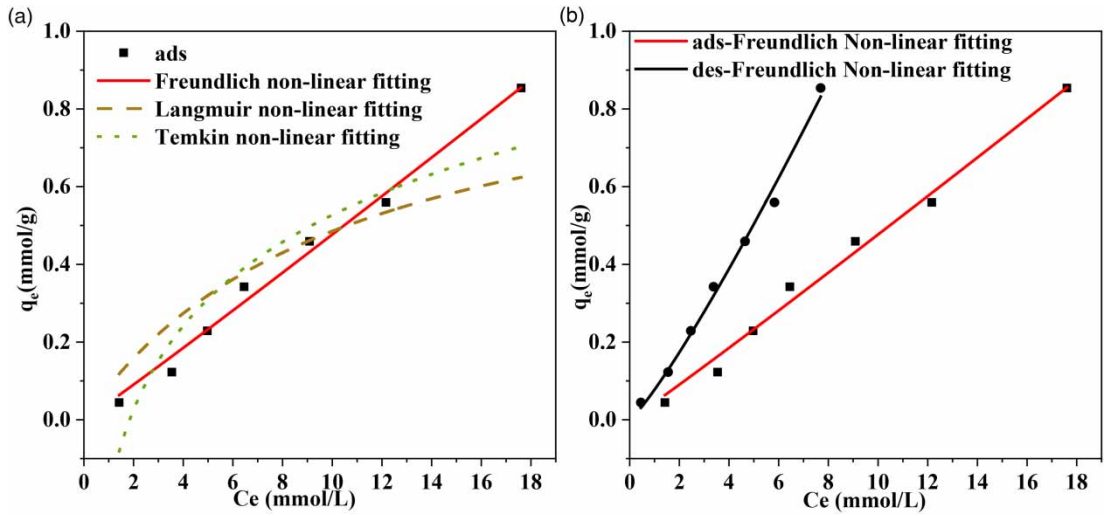

Figure 3 | (a) Non-linear fitting of Freundlich, Langmuir, and Temkin models for adsorption isotherms, (b) Non-linear fitting of the Freundlich model for adsorption and desorption isotherms. Conditions: 0.015 mol·L^{-1} NaCl, 200 rpm, 3 h, pH 3, AF_5 0.6 g/25 mL, 298 K.

Table 6 | Isothermal adsorption parameters of AF_5

Isotherm model	Parameters			
Langmuir	Q_m (mmol·L^{-1})	K_L (L·mmol^{-1})	R^2	Δqe (%)
	1	0.094	0.782	82.74
Freundlich	K_F (mg·g^{-1}) (L·mmol^{-1})$^{-1/n}$	$1/n$	R^2	Δqe (%)
	0.044	1.033	0.987	22.99
Temkin	K_L (L·mmol^{-1})	b_T (kJ·mol^{-1})	R^2	Δqe (%)
	0.543	7.952	0.856	119.98

results are shown in Table 6. The correlation coefficient (R^2) obtained by the Freundlich model reached 0.987, larger than the values for the Langmuir and Temkin models, and the Freundlich model was fitted with a smaller Δq_e, indicating that the adsorption of acetic acid onto AF_5 was dominated by multilayer adsorption and the adsorption surface is uneven (Ma *et al.* 2019). And the $1/n$ was larger than 1, exhibiting an S-type isotherm.

3.4. Desorption isotherm

Next, desorption experiments were performed to investigate the adsorption behavior and the desorption ability of pollutants on AF_5. These experiments with 0.015 mol/L NaCl were carried out under the same condition of adsorption isotherm experiments. AF_5 has been used in adsorption isotherm experiments and was re-added into a 0.015 mol/L NaCl solution. The desorption property of the adsorbent was analyzed using the Freundlich model (Figure 3(b)). The non-linear fitting results are as shown in Table 7, Freundlich's model can well explain the desorption process of acetic acid on AF_5, the R^2 was above 0.992.

A significant difference between the adsorption and desorption isotherm curves indicates that the desorption process is not a reversible process of adsorption and there is an obvious hysteresis effect (Figure 3(b)). Here the hysteresis coefficient is

Table 7 | Isothermal desorption parameters of AF_5

Isotherm model	Freundlich			
Parameters	K_F (mg·g^{-1}) (L·mmol^{-1})$^{-1/n}$	$1/n_{des}$	R^2	ΔC_e (%)
	0.077	1.164	0.992	15.36

defined as the ratio of the adsorption strength ($1/n$), expressed as $HI = (1/n_{des})/(1/n_{ads})$ (where n and n_{des} present the constants during the adsorption and desorption process fitted by the Freundlich model) (Hu *et al.* 2021).

When $HI < 0.7$, the desorption rate is slower than the absorption rate, which is a positive hysteresis, meaning acetic acid has a strong and irreversible interaction on AF_5. When $0.7 < HI < 1.0$, the desorption rate is similar to the adsorption rate, and the adsorption and desorption isotherms coincide with no hysteresis. When $HI > 1.0$, it is negative hysteresis, meaning a weak interaction between adsorbent and adsorbate. By the fitted parameter values of the adsorption and desorption process, the HI of acetic acid on AF_5 at 298 K was calculated to be 1.127, indicating a weak interaction between AF_5 and acetic acid, and an easy desorption advantage of AF_5. This means that simply washing with water can realize the elution and regeneration of AF_5, which is beneficial to the application of AF_5 in the acetic acid adsorption process and can effectively reduce the regeneration cost of the adsorbent.

3.5. Adsorption regeneration experiments

Considering the economy and environmental friendliness, the effective regeneration and stable adsorption performance of the adsorbent are important parameters for the wider application of the adsorbent in the adsorption process (Spessato *et al.* 2019). The regeneration of AF_5 was achieved through a lye elution at room temperature for 3 h, using 4 wt% of NaOH as the eluent. After elution, the used AF_5 was washed with deionized water to neutral, and then dried at 80 °C for 12 h. The adsorption efficiency after each regeneration is shown in Figure 4. Compared with coconut shell activated carbon, AF_5 had a better removal effect of acetic acid under the same conditions due to its larger specific surface area and different surface properties. After five successive adsorptions and elution cycles, the adsorption capacity of the AF_5 slightly decreased to ~88% of the initial adsorption capacity. Thus the AF_5 showed good regenerative adsorption properties. There were two reasons, firstly the easy desorption of acetic acid by AF_5 was verified by the desorption experiments, and the acetic acid adsorbed on AF_5 can neutralize with the lye, achieving effective desorption of acetic acid under a concentration gradient between the surface of adsorbent and solution. Secondly, the lye can largely increase the pH of the adsorption environment. In an alkaline environment, the adsorption effect of AF_5 is almost zero, verified by the pH influence experiment.

3.6. Treatment of actual wastewater

Finally, AF_5 was used to treat actual wastewater (COD = 846 mg·L^{-1}) obtained from catalytic wet air oxidation (CWAO) effluent, NAE Plant of Formosa Plastics Acrylate Ningbo Co., Ltd. Figure 5 shows the continuous adsorption–elution experiments performed with the actual wastewater. The continuous adsorption curve shows that AF_5 has a COD removal rate of 100% for the actual wastewater < 35 h (Figure 5(a)), the effluent from the CWAO/adsorption process reached discharge standard. After that, the adsorption effect decreased gradually, and finally (>50 h), the adsorbent reached saturation. In the continuous elution experiments, the AF_5 was completely eluted within 8 hours with a 0.8 wt% NaOH solution (Figure 5(b)). These results indicated that AF_5 can effectively remove pollutants from the wastewater in the AOP and it is a promising adsorbent with easy elution.

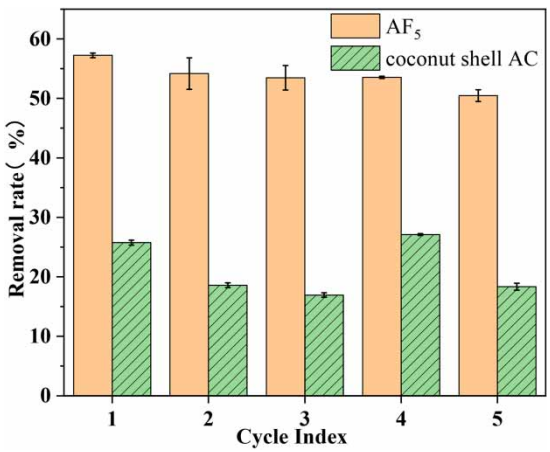

Figure 4 | Adsorption efficiency of regeneration experiments.

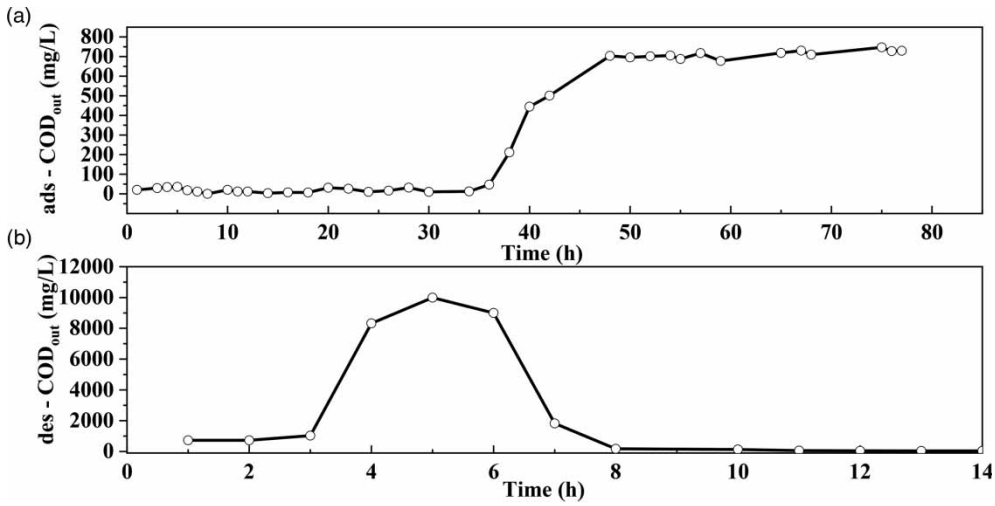

Figure 5 | Continuous adsorption–elution curve of AF_5 for actual CWAO wastewater. (a) Continuous adsorption curve. (b) Continuous elution curve. Conditions: $AF_5 = 50$ mL, pH $= 1.5 \pm 0.1$, flow speed $= 1\ h^{-1}$.

3.7. Adsorbent characteristic

3.7.1. Morphology and chemical composition

SEM was applied to study the AF_5's morphology, surface roughness, and particle size. Its internal pore structure information also can be analyzed by SEM of the cross-section. The SEM images showed that AF_5 has a uniform spherical shape with a ~600 μm particle size (diameter) (Figure 6(a)). The surface is relatively smooth with large cracks and pore structures, and a many disordered microcrystalline structures on the surface (Figure 6(b)). The cross-section shows some relatively uniform pores with uniform distribution (Figure 6(c) and 6(d)).

The SEM images of AF_5-5^{th} are shown in Figure 7. The adsorbent structure remains stable and the sphericity is maintained after five cycles, shown in Figure 7(a), indicating the structural stability of AF_5. There are salt particles in the pores on the

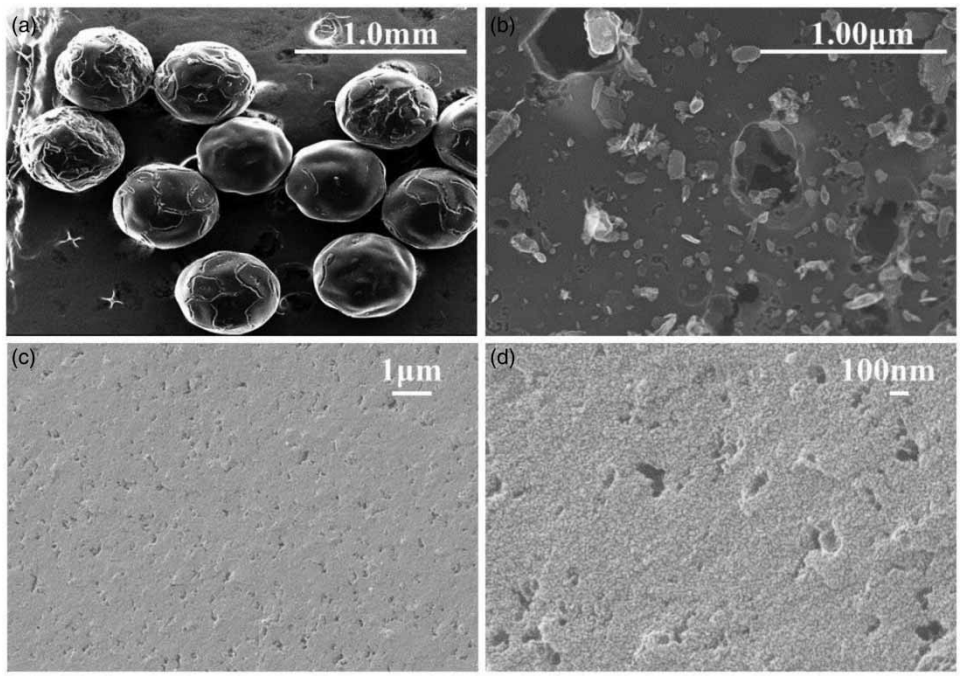

Figure 6 | SEM images of AF_5 surface and cross-section. (a, b) Surface morphology of AF_5 at different scales. (c, d) Morphology characteristics of AF_5 cross-section at different scales.

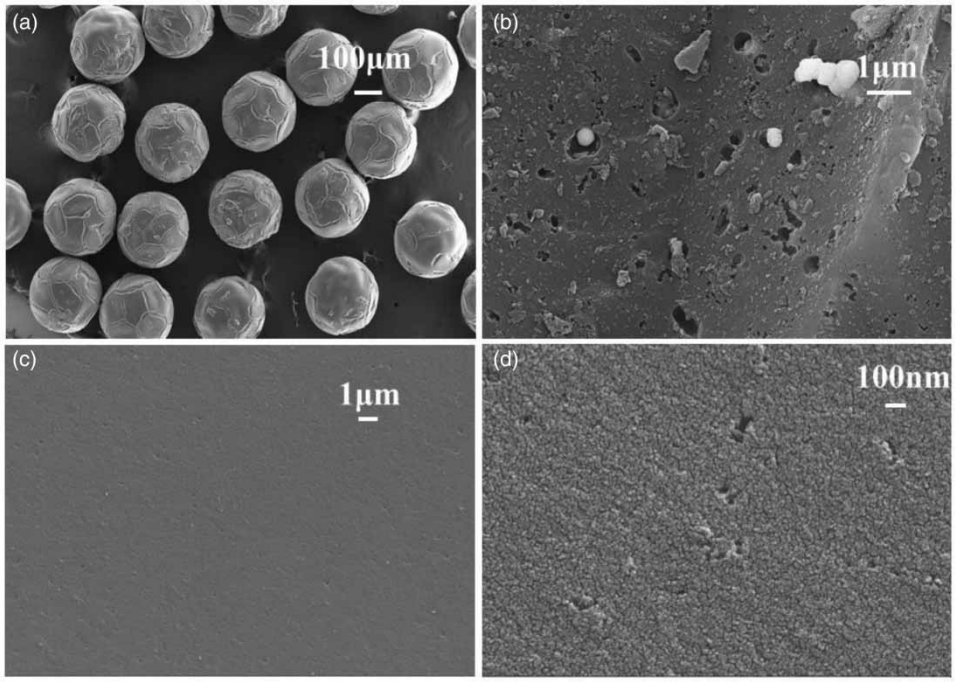

Figure 7 | SEM images of AF_5-5th surface and cross-section. (a, b) Surface morphology of AF_5-5th at different scales. (c, d) Morphology characteristics of AF_5-5th cross-section at different scales.

surface, shown in Figure 7(b), presumed to be sodium acetate formed by the reaction of acetic acid and NaOH after alkali regeneration. From the SEM image of the adsorbent cross-section shown in Figure 7(c) and 7(d), there are small-sized pores without salt particles, indicating that the sodium acetate produced by acid–base neutralization mostly exists on the surface of the AF_5.

Next, the crystalline property of AF_5 was measured by XRD in the range $2\theta = 10$–$90°$. Figure 8(a) shows that the diffraction peaks coexist with a broad diffraction curve, indicating the coexistence of both the crystalline phase and the amorphous phase (Sun *et al.* 2018). The broad diffraction peaks at $2\theta = 22.6°$, 43.6° and 79.5° corresponded to the (002) and (10) (overlapped 100 and 101) diffraction of disordered stacking of graphene layers, respectively (Saad *et al.* 2019). It is very consistent with the SEM results. According to Bragg's law, the interlayer spaces between adjacent carbon sheets are around 0.384 nm, which is larger than that of graphite (0.335 nm), indicating a non-graphitized carbonaceous structure.

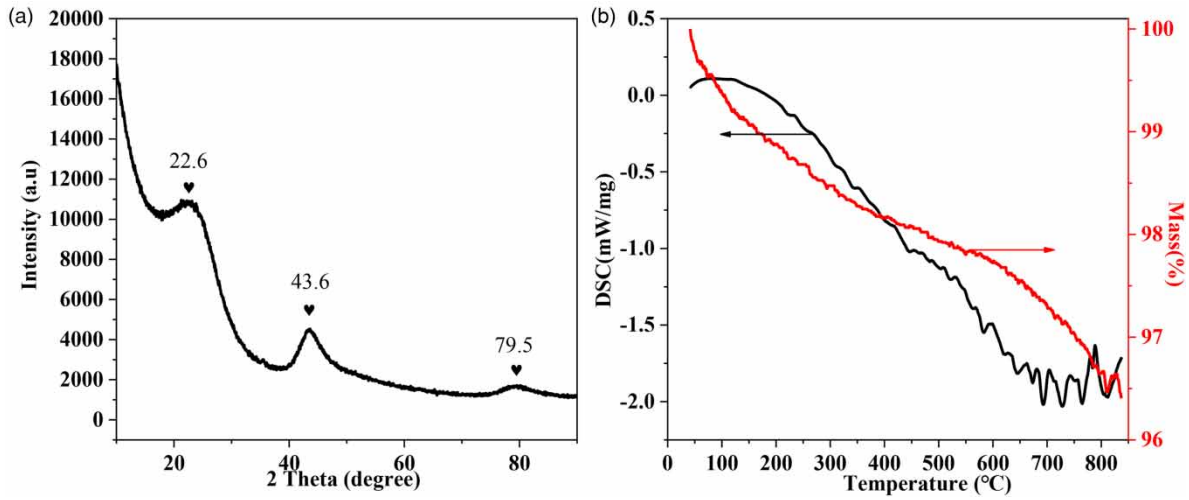

Figure 8 | (a) XRD analysis, (b) TG/DSC graph of AF_5.

The stability and composition of the adsorbent were analyzed by TG/DSC, the results are shown in Figure 8(b). The weight loss of AF_5 was ~3.5% in the temperature range of 40–840 °C, and the DSC curve had no obvious endothermic/exothermic peak. The results above indicated the great thermal stability of AF_5.

3.7.2. Specific surface area and pore size distribution

The specific surface area of adsorbents is directly related to the maximum capacity (amount of pollutants per gram of adsorbent), while the adsorption strength is inversely proportional to the pore size. The AF_5 and AF_5-5^{th} samples were characterized by N_2 adsorption–desorption. Figure 9(a) shows that AF_5 has both type-I and type-IV adsorption isotherms. At the beginning, there is a microporous adsorption process. At the medium pressure zone, a certain amount of adsorption and hysteresis occurs, meaning some mesopores. At the $P/P_0 = 0.4$, the hysteresis loop is closed, indicating that these mesopores are small. The specific surface area and pore size distribution of AF_5 can be obtained according to the NLDFT model. And the micropore volume of AF_5 is achieved by the t-plot method. The total pore volume is determined by the highest point of the N_2 adsorption isotherm, and the relevant pore parameters are given in Table 8. It was found that AF_5 is mainly a microporous structure with a relatively uniform pore size distribution, which is confirmed by the pore size distribution via the NLDFT model, shown in Figure 9(a) inset. Overall the excellent acetic acid adsorption performance of AF_5 can be mainly attributed to its rich microporous structure and large specific surface area.

The adsorption–desorption isotherm of AF_5-5^{th} was tested, shown in Figure 9(b). The type of adsorption isotherm of AF_5-5^{th} was similar to that of the fresh AF_5 samples. The pore size distribution of AF_5-5^{th} was still uniform, and its pore characteristic did not change significantly (Table 8), indicating the high stability of adsorbent.

3.8. Adsorption mechanism

FTIR was used to analyze the changes in the functional groups, the results are shown in Figure 10. AF_5-adsorbed refers to the sample prepared by dropping pure acetic acid onto the AF_5 powder. Only the -CH_3 vibration peak at 1,335 cm^{-1} can be confirmed, and no other functional group peaks could be observed for AF_5. The increasing pyrolysis temperature led to the

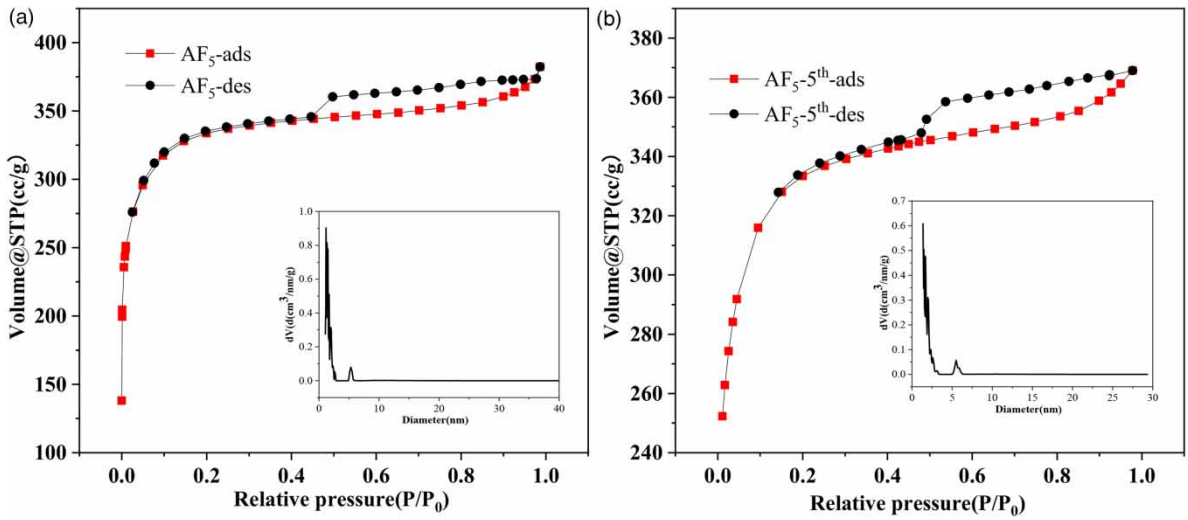

Figure 9 | N_2 adsorption–desorption isotherms and NLDFT pore size distribution of (a) AF_5, (b) AF_5-5^{th}.

Table 8 | Pore structure distribution of AF_5 and AF_5-5^{th}

Sample	S_{BET} ($m \cdot g^{-1}$)	V_{Total} ($cm^3 \cdot g^{-1}$)	Average pore size (nm)	$V_{Meso+Macro}$ ($cm^3 \cdot g^{-1}$)	V_{Micro} ($cm^3 \cdot g^{-1}$)	R ($V_{meso+macro}/V_{Micro}$)
AF_5	1,513	0.593	1.169	0.088	0.504	0.175
AF_5-5^{th}	1,582	0.571	1.368	0.083	0.488	0.170

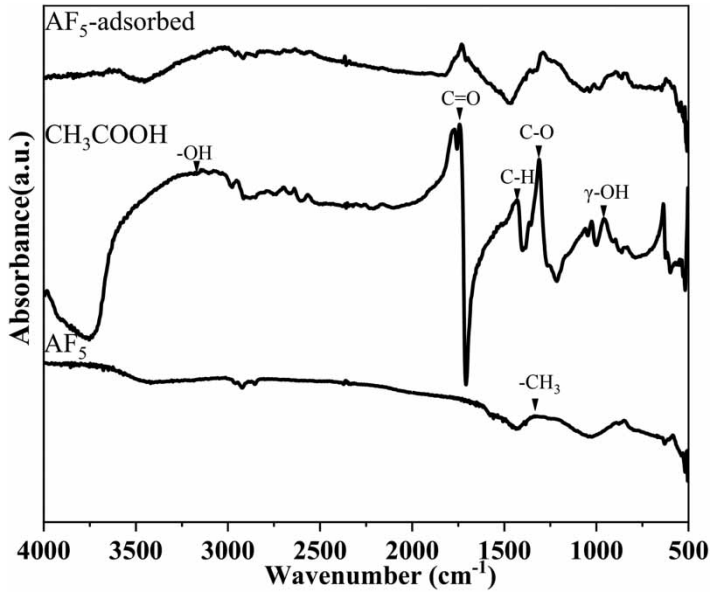

Figure 10 | FTIR analysis of AF_5, acetic acid and AF_5-adsorbed materials.

continuous increase in carbon during the high-temperature pyrolysis process for the material preparation. Therefore, the aromaticity increases continuously, and the functional groups on the surface of AF_5 gradually peel off (Zhang *et al.* 2018), which is consistent with the results from XRF. For acetic acid, the vibration peaks at 3,120 cm^{-1}, 1,739 cm^{-1}, 1,429 cm^{-1}, 1,312 cm^{-1} and 959 cm^{-1} represent -OH, C = O, $-CH_3$, C-O and γ-OH respectively. For AF_5-adsorbed material, the infrared spectrum is the superposition of AF_5 and acetic acid without new peaks appear, indicating that no chemical reaction occurred during the adsorption process.

The adsorption mechanism of AF_5 for acetic acid is exhibited in Figure 11. Combining the adsorption experiment and the characterization results above, the adsorption process perhaps included multiple aspects. First, the pore-filling effect can

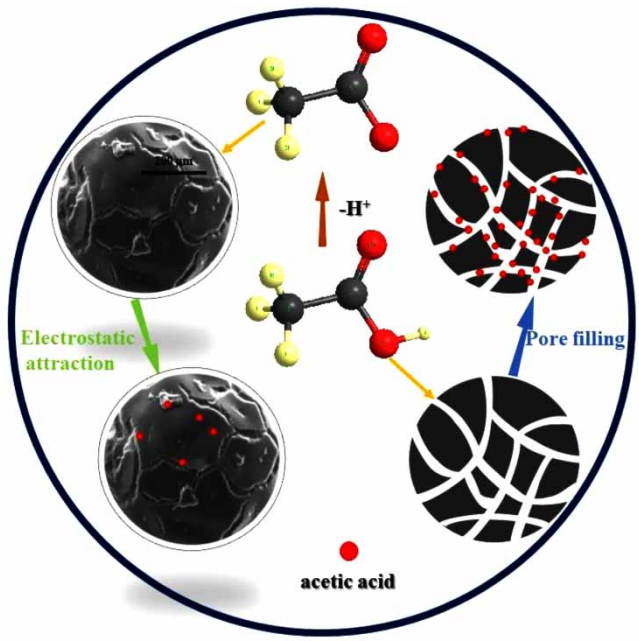

Figure 11 | The adsorption mechanism of AF_5 for acetic acid.

occur in enough pores of AF_5 to adsorb acetic acid efficiently. Secondly, electrostatic attraction between AF_5 and acetic acid was present. Under the higher pH solution, the surface of AF_5 had more negative charges, resulting in stronger electrostatic repulsion between the CH_3COO^- and the surface of AF_5.

4. CONCLUSIONS

In this work, we studied the acetic acid adsorption performance of resin-based spherical activated carbon AF_5. AF_5 has great advantages (adsorption performance) over other adsorbents, due to its abundant microporous structure and large specific surface area. The kinetic model results show that the adsorption process corresponds to the pseudo-second-order kinetic model. The adsorption kinetic is liquid-film controlled, confirmed by the intraparticle diffusion model. The adsorption process conformed to the Freundlich model and tended to multimolecular layer adsorption, the adsorption capacity increased with the increasing adsorbent concentration. Desorption experiments show a hysteresis between AF_5 and acetic acid, and the adsorption of acetic acid on AF_5 is mainly a physical adsorption process.

AF_5 exhibits good recyclability after the regeneration by simple elution, which is due to the intact pore characteristics. For actual factory wastewater, AF_5 also gives good adsorption-regeneration performance by simple elution, which has certain guiding significance for industrial applications.

The discussion on the adsorption mechanism according to the characterization of AF_5 is conducive to the development of similar alternative products, so as to further reduce the cost of adsorbents. It also provides a scientific basis for the application of RSAC in the AOPs coupled adsorption process to meet the standard discharge of industrial wastewater.

ETHICS APPROVAL AND CONSENT TO PARTICIPATE

Not applicable.

CONSENT FOR PUBLICATION

Not applicable.

AVAILABILITY OF DATA AND MATERIALS

The data supporting the findings of this study are available within the article. All other relevant source data are available from the corresponding author upon reasonable request.

COMPETING INTERESTS

The authors declare that they have no competing interests.

FUNDING

This work was supported by the National Key Research and Development Program of China (Grant no. 2019YFA0705803), the Strategic Priority Research Program of the Chinese Academy of Sciences (XDA21021101).

AUTHORS' CONTRIBUTIONS

CL.S supervised the progress of entire project. HL.W initiated the project and conceived the experiments, WJ.S; HZ.W; Y.Z; CY.J gave important suggestions on experiment designing and paper writing. X.Y and X.R gave important suggestions on experience device. All authors read and approved the final manuscript.

ACKNOWLEDGEMENTS

The authors thank Professor Wenjie Shen and Professor Gao Li (Dalian Institute of Chemical Physics) for their contribution. This work was supported by the National Key Research and Development Program of China (Grant no. 2019YFA0705803), the Strategic Priority Research Program of the Chinese Academy of Sciences (XDA21021101).

DATA AVAILABILITY STATEMENT

All relevant data are included in the paper or its Supplementary Information.

REFERENCES

Akbari, A., Sadani, M., Amin, M. M., Teimouri, F., Khajeh, M., Mahdavi, M. & Hadi, M. 2018 Managing sulfate ions produced by sulfate radical-advanced oxidation process using sulfate-reducing bacteria for the subsequent biological treatment. *Journal of Environmental Chemical Engineering* **6** (5), 5929–5937.

Amor, C., Marchao, L., Lucas, M. S. & Peres, J. A. 2019 Application of advanced oxidation processes for the treatment of recalcitrant agro-industrial wastewater: a review. *Water* **11** (2), 205.

Cherkasov, N. 2020 Liquid-phase adsorption: common problems and how we could do better. *Journal of Molecular Liquids* **301**, 112378.

Gonzalez, T., Dominguez, J. R. & Correia, S. 2020 Neonicotinoids removal by associated binary, tertiary and quaternary advanced oxidation processes: synergistic effects, kinetics and mineralization. *Journal of Environmental Management* **261**, 110156.

He, C., Men, G. S., Xu, B. T., Cui, J. & Zhao, J. L. 2017 Phenolic resin-derived activated carbon-supported divalent metal as efficient adsorbents (M-C, M = Zn, Ni, or Cu) for dibenzothiophene removal. *Environmental Science and Pollution Research* **24** (1), 782–794.

Herbert, A., Kumar, U. & Janardhan, P. 2020 Removal of hazardous dye from aqueous media using low-cost peanut (Arachis hypogaea) shells as adsorbents. *Water Environment Research* doi: 10.1002/wer.1491. Epub ahead of print.

Hu, M., Liu, L., Hou, N., Li, X., Zeng, D. & Tan, H. 2021 Insight into the adsorption mechanisms of ionizable imidazolinone herbicides in sediments: kinetics, adsorption model, and influencing factors. *Chemosphere* **274**, article number:129655.

Kameda, T., Horikoshi, K., Kumagai, S., Saito, Y. & Yoshioka, T. 2020 Adsorption of urea, creatinine, and uric acid onto spherical activated carbon. *Separation and Purification Technology* **237**, 116367.

Liang, Q. W., Luo, H. J., Geng, J. J. & Chen, J. D. 2018 Facile one-pot preparation of nitrogen-doped ultra-light graphene oxide aerogel and its prominent adsorption performance of Cr(VI). *Chemical Engineering Journal* **338**, 62–71.

Ma, L. F., Peng, F. Y., Li, H. P., Wang, C. Y. & Yang, Z. G. 2019 Adsorption of geosmin and 2-methylisoborneol onto granular activated carbon in water: isotherms, thermodynamics, kinetics, and influencing factors. *Water Science and Technology* **80** (4), 644–653.

Naidu, H. & Mathews, A. P. 2019 Simple methods for the determination of adsorption rate and equilibrium parameters in the recovery of acetic acid using GAC and synthetic resins. *Journal of Chemical & Engineering Data* **64** (12), 5705–5715.

Saad, M. J., Chia, C. H., Zakaria, S., Sajab, M. S., Misran, S., Rahman, M. H. A. & Chin, S. X. 2019 Physical and chemical properties of the rice straw activated carbon produced from carbonization and KOH activation processes. *Sains Malaysiana* **48** (2), 385–391.

Sanchez-Montes, I., Wachter, N., Silva, B. F. & Aquino, J. M. 2020 Comparison of UVC-based advanced oxidation processes in the mineralization of bisphenol A: identi fication of oxidation by products and toxicity evaluation. *Chemical Engineering Journal* **386**, 123986.

Shi, J. X., Huang, W. P., Han, H. J. & Xu, C. Y. 2020 Review on treatment technology of salt wastewater in coal chemical industry of China. *Desalination* **493**, 9.

Spessato, L., Bedin, K. C., Cazetta, A. L., Souza, I. P. A. F., Duarte, V. A., Crespo, L. H. S., Silva, M. C., Pontes, R. M. & Almeida, V. C. 2019 KOH-super activated carbon from biomass waste: insights into the paracetamol adsorption mechanism and thermal regeneration cycles. *Journal of Hazardous Materials* **371**, 499–505.

Sun, Q. Q., Zhao, X. K., Wang, D. M., Dong, J. N., She, D. & Peng, P. 2018 Preparation and characterization of nanocrystalline cellulose/*Eucommia ulmoides* gum nanocomposite film. *Carbohydrate Polymers* **181**, 825–832.

Sun, W. J., Wei, H. Z., An, L. Y., Jin, C. Y., Wu, H. L., Xiong, Z. A., Pu, C. Y. & Sun, C. L. 2019 Oxygen vacancy mediated La1-xcexfeo3-δ perovskite oxides as efficient catalysts for CWAO of acrylic acid by A-site Ce doping. *Applied Catalysis B: Environmental* **245**, 20–28.

Tagliavini, M., Engel, F., Weidler, P. G., Scherer, T. & Schafer, A. I. 2017 Adsorption of steroid micropollutants on polymer-based spherical activated carbon (PBSAC). *Journal of Hazardous Materials* **337**, 126–137.

Wang, Y. M., Wei, H. Z., Zhao, Y., Sun, W. J. & Sun, C. L. 2017 The optimization, kinetics and mechanism of m-cresol degradation via catalytic wet peroxide oxidation with sludge-derived carbon catalyst. *Journal of Hazardous Materials* **326**, 36–46.

Wang, M. M., Wen, B. Y., Fan, B. M. & Zhang, H. J. 2020 Study on adsorption mechanism of silicate adsorbents with different morphologies and pore structures towards formaldehyde in water. *Colloids and Surfaces A-Physicochemical and Engineering Aspects* **599**, 9.

Yang, J. B., Ling, L. C., Liu, L., Kang, F. Y., Huang, Z. H. & Wu, H. 2002 Preparation and properties of phenolic resin-based activated carbon spheres with controlled pore size distribution. *Carbon* **40** (6), 911–916.

Yu, C., Liu, H., Lyu, J., Xiao, Z., Bai, P. & Guo, X. 2019 Tuning adsorption capacity by alkoxy groups: a study on acetic acid adsorption on UiO-66 analogues from aqueous solution. *Industrial & Engineering Chemistry Research* **58** (27), 12272–12279.

Zhang, H., Lan, X., Bai, P. & Guo, X. 2016 Adsorptive removal of acetic acid from water with metal-organic frameworks. *Chemical Engineering Research and Design* **111**, 127–137.

Zhang, C. M., Song, W., Zhang, X. C., Li, R., Zhao, S. J. & Fan, C. M. 2018 Synthesis, characterization and evaluation of resin-based carbon spheres modified by oxygen functional groups for gaseous elemental mercury capture. *Journal of Materials Science* **53** (13), 9429–9448.

First received 26 April 2021; accepted in revised form 11 June 2021. Available online 25 June 2021